J. Phys. B: At. Mol. Opt. Phys. 22 (1989) 1175–1181. Printed in the UK

Study of anomalous dispersion in elastic scattering of 59.5 keV photons at K-absorption edges of target atoms

S S Nandi†, S K Ghose, S K Sengupta‡ and N Chaudhuri
Department of Physics, University of North Bengal, Darjeeling, India

Received 10 February 1988, in final form 25 October 1988

Abstract. Elastic scattering cross sections of photons at large angles for target atoms with K-absorption edge energy near 59.5 keV have been calculated using the anomalous dispersion model. The results calculated for representative target atoms have been compared with the results obtained from exact numerical partial-wave methods of Kissel and coworkers and our new experimental results.

1. Introduction

An investigation to examine dispersion in elastic scattering of photons near K-absorption edges of target atoms has been undertaken in view of the fact that exact numerical partial-wave cross sections in the model of Kissel *et al* (1986) are not yet available at all K-shell threshold energies of target atoms near 59.5 keV. We have applied a dispersion relation known as the Kramers–Kronig relation with the optical theorem to obtain differential elastic scattering cross sections near K-shell threshold energies, and have compared these theoretical results with our experimental results on several target atoms, particularly on $_{68}$Er whose K-edge energy is very close to 59.5 keV. Similar investigations have been published by Schumacher and Stoffregen (1977). However, there are differences between our work and the previous work of Schumacher and Stoffregen (1977) in respect of target atoms and scattering angles and the evaluation of anomalous dispersion factors. In the previous work the trend of the dispersion effect only at an angle of 150° was demonstrated and was compared with experimental results. But we have theoretically calculated the values of differential elastic scattering cross sections of photons of energy 59.5 keV for several target atoms at various large angles. Also we have compared the results with the calculated results of Kissel *et al* (1986) for common elements and scattering angle and also compared with our present experimental results. Several compilations of theoretical coherent photon–atom scattering factors are available for use in calculating the interactions of radiation with matter. We have used the values of real and anomalous scattering factors from compilations of Creagh and McAuley (1989) and values of relativistic atomic scattering factors (f_0) from the compilations of Hubbell and Overbo (1979).

† Guest researcher.
‡ University Service and Instrumentation Centre, North Bengal University.

0953-4075/89/081175+07$02.50

2. Experimental details

The experimental arrangement and the method used to measure the scattering cross sections at large angles are the same as those described in our earlier work (Nandi *et al* 1987). Only a schematic diagram of the experimental arrangement is shown in figure 1. The ^{241}Am (59.5 keV) source was placed in a lead housing of size 46 cm × 46 cm × 56 cm in order to ensure that no direct beam of gamma rays could enter the detector. The housing had a conical bore 30 cm in length and 2 cm in diameter.

While in our previous measurements (Nandi *et al* 1987) we tried to perform the whole set of experiments with scattering angle from 60° to 165° with the help of a single experimental set-up, in the present measurements a second set-up was designed for target element $_{68}$Er for scattering angles up to 135°. In this second set-up additional shielding provision has been made. The collimating system has been improved by increasing the thickness of the lead housing over that in the first set-up. The size of the lead housing in the second set-up for scattering angles up to 135° was 66 cm × 66 cm × 76 cm. The 30 cm long and 2 cm diameter bore conical beam collimating system remained unaltered.

The increased thickness of the lead housing could not be used for scattering angles 150° and 165° because the finite size of the liquid-nitrogen dewar of the germanium detector put a limit on the maximum thickness of the lead housing. The dimensions of the target foils are given in table 1.

A representative example of a scattered spectrum, illustrating the complete separation of coherent scattering from incoherent scattering, is given in figure 2.

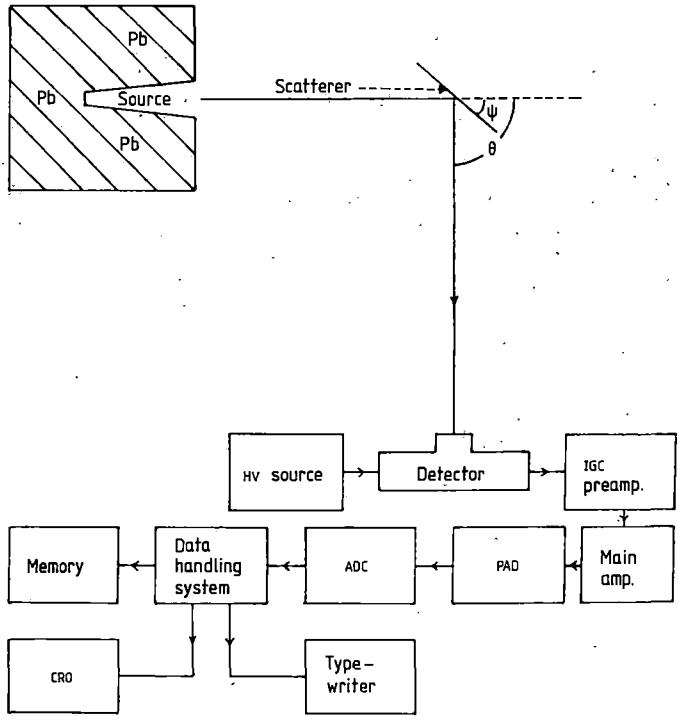

Figure 1. Experimental arrangement.

Table 1. Target foil dimensions.

Target atom	Area (cm^2)	Thickness (cm)
Mo	25	0.01
Sn	19.63	0.01
Cd	25	0.005
Er	25	0.01

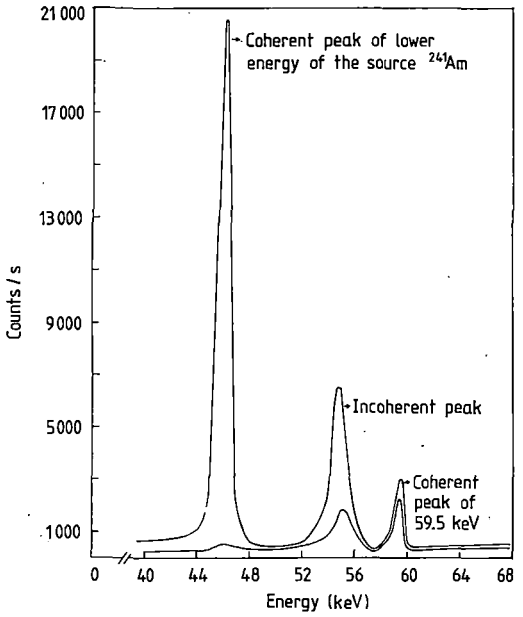

Figure 2. Spectrum of 59.5 keV photons scattered by Er through an angle $\theta = 60°$ (upper curve) and empty target background (lower curve).

3. Errors

The error arising from the superposition of coherent and incoherent peaks in the scattered spectrum was completely eliminated, as is evident from an inspection of figure 2. Possible systematic and random errors have been taken into consideration in the evaluation of the measured differential cross sections. The systematic errors include uncertainties in the determination of the photo-peak area of the scattered spectra and uncertainties due to a variation in the detector background in the presence and absence of sample materials. Sources of random errors include statistical uncertainty in counting and uncertainties in measuring sample sizes, angles and distances. Systematic errors have either been excluded effectively or accounted for with appropriate corrections. Owing to the finite size of the scatterer the error arising in measuring a certain scattering angle is negligible (e.g. $\Delta\theta = \pm 0.25°$ for $\theta = 135°$) since the angular width of the incident photon beam on the target of finite size is very small (8°). The corresponding error in $d\sigma/d\Omega$ is ± 0.004 b sr^{-1}, which is also negligible. The errors are in the range of about 4–9%.

4. Results

Results from the set of measurements using 59.5 keV photons are shown in figure 3 and are also presented in table 2 together with experimental errors and recent theoretical and experimental data at the same energy. In table 3 results of the theoretical differential cross sections, calculated in the dispersion model, are presented.

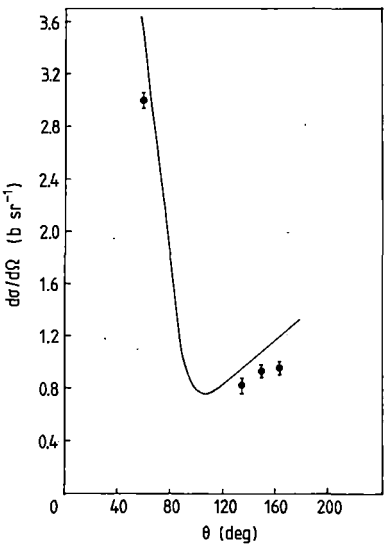

Figure 3. Differential elastic scattering cross sections of Er computed with the help of dispersion theory compared with experimental results at different scattering angles: ——, our theoretical results; ●, present measurements.

5. Discussion

The whole photon–atom differential elastic scattering cross section is expressed simply as

$$d\sigma/d\Omega = \tfrac{1}{2}r_0^2|f|^2(1+\cos^2\theta) \tag{1}$$

where f is the atomic scattering factor, $r_0 = e^2/mc^2$ is the classical electron radius and θ is the scattering angle. The atomic scattering factor is defined as

$$f = f_0(q) + \Delta f' + i\Delta f''. \tag{2}$$

The atomic scattering factor for a radial charge number density is

$$f_0(q) = 4\pi \int_0^\infty \rho(r) \frac{\sin(qr)}{(qr)} r^2 \, dr \tag{3}$$

and

$$\hbar q = 2(\hbar\omega/c)\sin(\theta/2) \tag{4}$$

Table 2. Comparison of our theoretical results of differential elastic scattering cross sections with experimental results and theoretical results of Kissel *et al* (1986).

		$d\sigma/d\Omega$ (b sr^{-1})			
		Theoretical			
Element	Scattering angle, θ (deg)	Our calc.	Kissel *et al* (1986)	Present expt	Expt results of Schumacher and Stoffregen (1977)
$_{42}$Mo	60	1.33	1.32	1.406 (±0.058)	1.28 (5)
	90	0.502	0.499	0.578 (±0.027)	0.513 (20)
	135	0.345	0.331	0.335 (±0.016)	0.341 (13)
	165	0.343	0.338	0.427 (±0.030)	-
$_{50}$Sn	60	1.86	1.86	1.78 (±0.076)	1.90 (8)
	90	0.819	0.824	0.826 (±0.040)	0.844 (34)
	135	0.677	0.661	0.687 (±0.033)	0.679 (25)
$_{48}$Cd	90	0.745	0.748	0.997 (±0.053)	
	135	0.585	0.568	0.810 (±0.040)	
	165	0.585	0.583	0.656 (±0.057)	
$_{68}$Er[a]	60	3.53		3.008 (±0.116)	
	135	0.993		0.824 (±0.032)	
	150	1.09		0.937 (±0.044)	
	165	1.16		0.967 (±0.074)	

[a] The results for $_{68}$Er particularly at angles 60° and 135° in our previous paper were different, presumably due to some uncertainty in scattering angle measurements and background effect.

Table 3. Calculated values of differential elastic scattering cross section for 59.5 keV photons.

		$d\sigma/d\Omega$ (b sr^{-1})					
θ (deg)	x (Å^{-1})	$_{54}$Xe (34.56)[a]	$_{63}$Eu (48.52)	$_{66}$Dy (53.79)	$_{68}$Er (57.49)	$_{70}$Yb (61.33)	$_{73}$Ta (67.42)
0	0	2.33 (+2)[b]	3.09 (+2)	3.33 (+2)	3.44 (+2)	3.590 (+2)	4.030 (+2)
30	1.24	1.59 (+1)	2.05 (+1)	2.10 (+1)	2.04 (+1)	2.000 (+1)	2.525 (+1)
60	2.40	2.079	3.533	3.709	3.53	3.002	4.415
90	3.39	0.832	1.135	1.104	1.02	0.533	1.038
120	4.16	0.682	0.993	0.938	0.827	0.255	0.602
135	4.42	0.733	1.109	1.054	0.993	0.256	0.632
150	4.63	0.761	1.203	1.151	1.090	0.246	0.640

[a] Figures in parentheses after element symbol indicate K-shell threshold energy values (keV).
[b] Figures in parentheses after cross section values mean powers of 10.

is the momentum transferred to the atom in the scattering process. In terms of linear photon polarisations, there exist two independent scattering amplitudes. We use the notation $A_{\parallel}^{R}$ and $A_{\perp}^{R}$ to indicate the scattering amplitudes for photons of polarisation parallel and perpendicular respectively to the plane of scattering. We may write the elastic scattering cross sections for scattering of unpolarised incident photons as

$$d\sigma/d\Omega = \tfrac{1}{2}(|A_{\perp}^{R}|^2 + |A_{\parallel}^{R}|^2). \tag{5}$$

Since the angular dependences of anomalous scattering factors are small at large angles, forward-angle ($\theta = 0$) anomalous scattering factors are used without modification at other angles. In terms of linear photon polarisations we can write

$$\begin{aligned} \text{Re } A_{\perp}^{R} &= -(f_0 + \Delta f') & \text{Re } A_{\parallel}^{R} &= (\text{Re } A_{\perp}^{R}) \cos\theta \\ \text{Im } A_{\perp}^{R} &= -\Delta f'' & \text{Im } A_{\parallel}^{R} &= (\text{Im } A_{\perp}^{R}) \cos\theta. \end{aligned} \tag{6}$$

In the case of forward-angle scattering $\Delta f''$ is given by the optical theorem as

$$\Delta f''(\omega) = \frac{\omega}{4\pi r_0 c}\sigma_{\text{ph}}(\omega)$$

and $\Delta f'$ by the classical dispersion theory as

$$\Delta f'(\omega) = \frac{1}{2\pi^2 r_0 c}\,\text{P}\int_{\omega_k}^{\infty} \frac{\omega'^2 \sigma_{\text{ph}}(\omega')}{\omega^2 - \omega'^2}\,\text{d}\omega' \tag{7}$$

where $\sigma_{\text{ph}}(\omega)$ is the photoelastic cross section and P indicates the principal value of the integral.

In calculating the theoretical values of differential elastic scattering cross sections we have used the values of relativistic atomic scattering factors (f_0) compiled by Hubbell and Overbo (1979) and the values of anomalous scattering factors as compiled by Creagh and McAuley (1989). Our computed differential cross section results based on dispersion theory and experimental cross section results are compared with the computations of Kissel *et al* (1986) based on an exact numerical partial-wave method within the independent-electron model of the atom, in table 2. A study of table 2 shows that, although certain assumptions are involved in our calculation in the dispersion model, excellent agreement exists between our computed results based on dispersion theory and the modern computer-aided rigorous calculations of Kissel *et al* (1986). As an easy and ready method for calculating the differential elastic scattering cross sections of different target elements at different scattering angles, the technique based on the dispersion model is an adequate one even when exact results in the model of Kissel *et al* (1986) are not available for target atoms of interest. This has happened in the case of $_{68}$Er with K-shell binding energy 57.49 keV in the present work, which has demonstrated the usefulness of calculations based on the dispersion model particularly at K-shell threshold energies. Some theoretical results of differential elastic scattering cross sections of representative target atoms from our ongoing research programmes have been included in this paper. A closer study of table 2 shows that theoretical and experimental results agree with each other better when scattering angles are very large (for example 150° and 165°) and in cases where the K-edge energy of the target element is closer to the incident photon energy, as in the case of $_{68}$Er. This is also in accordance with the findings of Tirsell *et al* (1975). This again indicates that the dispersion effect is dominant when the incident photon energy is close to the K-edge energy of the target atoms and for large scattering angles. In figure 3 the results of the differential cross sections, computed with the help of dispersion theory, are plotted at different angles for the target element $_{68}$Er together with our experimental data points. Within the limits of the experimental errors and theoretical approximations, data points follow the general trend of the theoretical curve. The trend of the variation of the 59.5 keV photon differential cross section with atomic number of the target atoms considered is shown with the present data points in figure 4. Further measurements to test such cross section variation at 59.5 keV have been undertaken by the present workers.

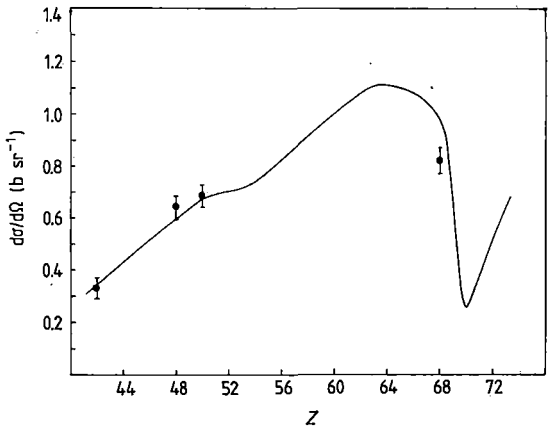

Figure 4. Variation of differential cross section of elemental targets for 59.5 keV photons at a scattering angle $\theta = 135°$: ——, theoretical curve; ●, experimental points.

Acknowledgments

The authors acknowledge the receipt of atomic scattering factor data from Dr J H Hubbell of the National Bureau of Standards, Washington, DC, and the receipt of data on dispersion corrections from Dr D C Creagh of University College of New South Wales. The award of a teacher fellowship to S K Ghose by the University Grants Commission is also acknowledged.

References

Creagh D C and McAuley W J 1989 *International Tables for Crystallography* vol C, § 4.2.6
Hubbell J H and Overbo I 1979 *J. Phys. Chem. Ref. Data* **8** 69–105
Kissel L, Kane P, Pratt R H and Roy S C 1986 *Phys. Rep.* **140** 75–159
Nandi S S, Dutta R and Chaudhuri N 1987 *J. Phys. B: At. Mol. Phys.* **20** 4027–33
Schumacher M and Stoffregen A 1977 *Z. Phys.* A **283** 18
Tirsell K G, Slivinsky V W and Ebert P J 1975 *Phys. Rev.* A **12** 2427

Small-angle scattering of photons at low energies

NANAK BHATTACHARYYA[1], S. K. GHOSE, AND N. CHOUDHURI
Department of Physics, University of North Bengal, Darjeeling, Pin 734430, India

Received July 7, 1986[2]

The results of a new set of photon–atom scattering measurements in a low momentum-transfer region (0.02–0.04 *mc*) for medium- and high-*Z* elemental scatterers in the form of foils are presented. A comparison with the theoretical results based on the Thomas–Fermi model for the incoherent scattering components and the numerical *S*-matrix predictions for the coherent Rayleigh-scattering amplitudes are also given. The present series of measurements fills a gap in the region of low momentum transfer that has not been covered by other recent scattering experiments.

On présente les résultats d'un nouvel ensemble de mesures sur la diffusion, dans la région des faibles transferts d'impulsion (0.02–0.04 *mc*), des photons par des atomes de *Z* moyen et élevé, les diffusers étant sous forme de feuillets, en même temps que des résultats théoriques basés sur le modèle Thomas–Fermi pour la composante de diffusion incohérente et sur les prédictions numériques de la matrice *S* pour les amplitudes de diffusion Rayleigh cohérente. Cette série de mesures vient combler un vide dans la région des faibles transfers d'impulsion que n'a pas été couverte par les autres expériences de diffusion effectuées récemment.

[Traduit par la revue]

Can. J. Phys. **66**, 987 (1988)

1. Introduction

The theoretical methods for calculating both coherent and incoherent scattering of low-energy photons in X-ray and γ-ray regions have recently been improved significantly. Very accurate results have been obtained through the use of modern computers. For example, the calculation of elastic photon scattering cross sections in the energy range 100 keV–10 MeV by Kissel and Pratt (1) are purported to be the best available so far. However, these calculations have not yet been tested at smaller scattering angles to cover a wide range of momentum transfer at lower photon energies. A new set of scattering measurements in the angular range 5°–20° has been carried out at a photon energy of 59.54 keV for intermediate- and high-*Z* elements to test the theories of both coherent and incoherent photon scattering processes at small angles.

2. Experimental arrangement for very small angle scattering

The typical small-angle geometry used in the experimental arrangement (shown in Fig. 1) permitted scattering measurements to be made at small angles that could not otherwise be measured, owing to the dead space caused by the straight primary photon beam from the source. The straight part of the conical primary beam was absorbed by the brass stopper, and the detector was completely within the shadow of the stopper. The fractional solid angle from the source–detector to the annular-ring scatterer was limited to the range $2.2 \times 10^{-3} - 8.5 \times 10^{-3}$ for a scattering angle range of 5°–20°. In the geometry shown, the distance between the source and scatterer and between the scatterer and the detector were both in the range 1–1.6 m. Annular scatterers with an outer diameter of 5 cm and a scattering width of ~1 cm had thicknesses in the range 0.01–0.10 mm. The ^{241}Am disc source that was used had an active diameter of 4.2 mm. The shieldings and the double-cone stopper, designed to minimize scattering from them, were arranged to reduce the detector background material within the geometry of the setup.

At a scattering angle of θ, the expression for the total (coherent + incoherent) differential scattering cross section is given by

$$\sigma(\theta) = \frac{C}{C_r} S \frac{A r^2}{NM} \exp(\mu t/\cos\phi)\ \mathrm{cm}^2 \cdot \mathrm{atm}^{-1} \cdot \mathrm{sr}^{-1}$$

C is the number of photons that are scattered by the scatterer per second at an angle θ; C_r is the mean number of photons detected per second from a similar weak reference source placed at different parts of the scatterer; *S* is the strength of the main source relative to the weak reference source; A is the atomic weight of the scatterer material; *N* is Avogadro's number; *r* (cm) is the source-to-scatter mean distance; *M* (g) is the mass of the scatterer; μ ($\mathrm{cm}^2 \cdot \mathrm{g}^{-1}$) is the attenuation coefficient of the scatterer material for incident primary photons; *t* ($\mathrm{g} \cdot \mathrm{cm}^{-2}$) is the thickness of the annular-ring scatterer; and φ is the mean angle between the lines joining the source to the scatterer and the source to the detector.

3. Experimental details

3.1. Measurement of the differential cross sections

The small-angle differential measurements were made using an ND 1100 multichannel analyzer system coupled to a 2.5 cm × 2.5 cm NaI(Tl) scintillation detector head at a conversion gain of 1024 with 512 channels and spectrum storage times in the range 4–100 ks. A ^{241}Am (59.54 keV; 10 mCi, 1 Ci = 37 GBq) source was used in the measurements on the following scattering atoms: copper, tin, silver, tantalum, gold, and lead. The scattering materials were very pure and in the form of thin foils; scattering counts were taken for a minimum of 10 ks. For example, at a scattering angle of 17.7° for the lead scatterer, the total count recorded was 7.00×10^6. The photons scattered at such small scattering angles could not be spectrally analyzed to separate the incoherent component, and total scattering counts only were determined with a statistical error of 1%.

3.2. Experimental cross section, corrections and errors

The measured differential cross sections at small angles (5°–20°) are presented in tabular form (Table 1) together with the theoretical results for the differential cross sections. The experimental results for Cu, Ag, Sn, Ta, Au, and Pb cover a momentum transfer range of 0.018–0.037 *mc*.

The corrections applied to the experimental cross-section data included (i) a sample-dependent background and (ii) the

[1]Also affiliated with University Bachelor of Training and Evening College, Cooch Behar, India.

[2]Revision received March 25, 1988.

Printed in Canada / Imprimé au Canada

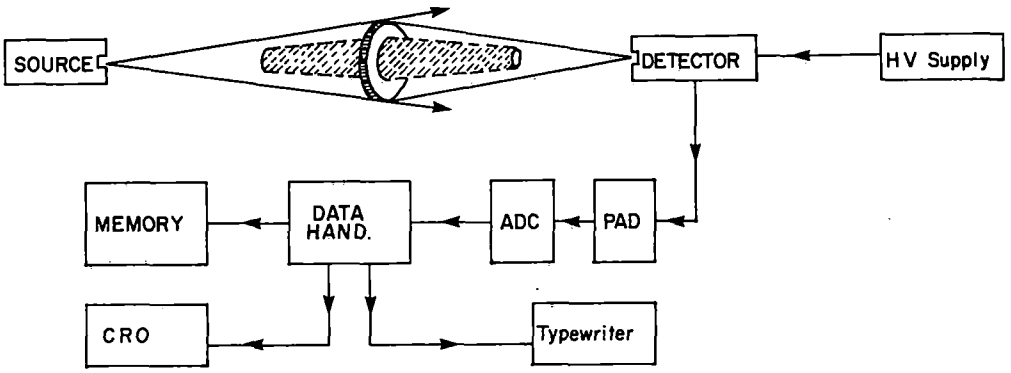

FIG. 1. Experimental arrangement for differential scattering cross-section measurements at low angles. Data hand, data handling system; ADC, analog-to-digital converter; PAD, pulse-amplitude discriminator; CRO, cathode ray oscilloscope; HV, high voltage.

TABLE 1. Measured differential scattering cross section $\sigma(\theta)$ ($b \cdot sr^{-1} \cdot atom^{-1}$)

Element	Scattering angle θ (deg)	q (mc)	$\sigma(\theta)_{inc}$	$\sigma(\theta)_{coh}$[a]	Theoretical total $\sigma(\theta)$	Experimental $\sigma(\theta)$
^{29}Cu	8.9	0.018	1.01[b] (0.79)[c]	23.67	24.68[b] (24.46)[c]	31.88±3.30
	12.6	0.023	1.18 (1.03)	13.48	14.66 (14.51)	16.89±1.69
	14.2	0.029	1.25 (1.13)	10.76	12.00 (11.89)	12.99±1.33
	17.7	0.036	1.35 (1.28)	6.81	8.16 (8.09)	8.26±0.98
^{47}Ag	8.9	0.018	1.35 (1.10)	65.15[d]	66.50[d] (66.25)[d]	71.19±7.41
	12.6	0.023	1.60 (1.45)	42.70	44.30 (44.15)	41.69±4.40
	14.2	0.029	1.71 (1.58)	35.48	37.19 (37.06)	37.08±4.01
	17.7	0.036	1.91 (1.74)	27.45	29.36 (29.19)	25.84±2.71
^{50}Sn	8.9	0.018	1.41 (1.16)	76.94	78.35 (78.10)	88.68±8.98
	12.6	0.023	1.64 (1.50)	50.18	51.82 (51.68)	52.49±5.39
	14.2	0.029	1.79 (1.64)	42.63	44.42 (44.27)	41.25±4.26
	17.7	0.036	1.97 (1.87)	31.23	33.20 (33.10)	31.44±3.31
^{73}Ta	8.9	0.018	1.78 (1.40)	180.51	182.29 (181.91)	297.25±30.43
	12.6	0.023	2.12 (1.84)	121.21	123.33 (123.05)	174.18±18.41
	14.2	0.029	2.24 (2.00)	102.54	104.78 (104.54)	124.37±13.23
	17.7	0.036	2.64 (2.27)	71.22	73.86 (73.49)	77.01±8.31
^{79}Au	5.7	0.012	1.36 (0.90)	311.55	312.91 (312.45)	336.17±34.55
	9.4	0.019	1.89 (1.48)	208.20	210.09 (209.68)	221.12±23.02
	13.2	0.027	2.28 (1.76)	142.69	144.97 (144.45)	137.31±14.61
	15.0	0.030	2.41 (2.18)	120.00	122.41 (122.18)	118.37±12.54
	18.6	0.038	2.70 (2.49)	86.71	89.41 (89.20)	84.83±9.34
^{82}Pb	8.9	0.018	1.88 (1.47)	238.87	240.75 (240.34)	238.46±24.82
	12.6	0.023	2.23 (1.95)	166.02	168.25 (167.97)	162.41±17.15
	14.2	0.029	2.41 (2.16)	142.85	145.26 (145.01)	151.45±16.38
	17.7	0.036	2.66 (2.71)	104.21	106.87 (106.92)	109.36±12.05

[a]Obtained from Rayleigh amplitudes calculated by the Pittsburgh group.
[b]Based on $S(q,Z)$ in the Thomas–Fermi model.
[c]Based on $S(q,Z)$ in the self-consistent field (SCF) calculations.
[d]Results of silver (Ag) based on $F(x,Z)$ in the nonrelativistic form factor formulation (5).

finite angular width at each scattering angle in the range 0.5°–2°. The former needed a correction of up to 5%. The sample-dependent background absorbed in the sample was obtained from $\sim B_s(1 - \mu t)$, where μ is the attenuation coefficient (2). B_s was found from the same measurements at two scatterer thicknesses, and the scattering counts were corrected accordingly. The correction for the angular spread was obtained by determining the form of the variation of the theoretical differential cross section with respect to the angle in the range 1°–20°; the correction was found to be within 3% for an angular spread of $\Delta\theta/\theta = \frac{1}{4}$.

Possible systematic and random errors have been taken into account in the evaluation of measured cross sections. These include uncertainties in (i) the determination of the photopeak area of the scattered spectra, (ii) the attenuation coefficients for 59.5 keV photons in the scatterer materials, (iii) the value of the relative source strength S, and (iv) the counting and measuring sample size and distances. Systematic errors have been either excluded effectively or accounted for with appropriate corrections. The activity of the main and reference sources had an uncertainty less than ±5%, and the attenuation coefficients for 59.5 keV photons were known to an accuracy of ~1%. The

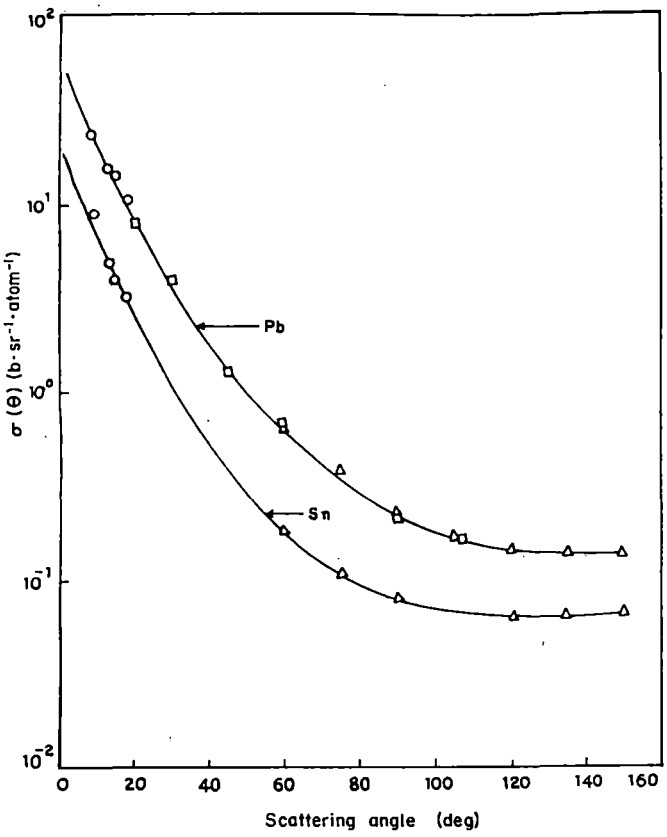

FIG. 2. Differential scattering cross sections of 59.54 keV photons. The results of the present measurements (○) are compared with the earlier measurements of Schumacher and Stoffregen (9) (△) and Eichler and de Barros (10) (□) and with the best theoretical values of Kissel (3) (—).

counting errors for most of the measurements were within 1%. Errors due to differences in sample size, etc. have been kept to a minimum in all measurements.

4. Theoretical scattering cross section

4.1. Coherent scattering cross section

At the photon energy in question, the elastic scattering of photons by bound atomic electrons (Rayleigh scattering) entirely dominates the scattering process. Very accurate numerical results for Rayleigh scattering are now available from the most recent extensive numerical computation of Rayleigh-scattering amplitude data by Kissel (3). Many of these results, which have not yet been experimentally tested, are used in the present analysis; see Table 1.

4.2. Incoherent scattering cross section

In the absence of an exact theory of incoherent (INC) scattering for a heavy atom, the effect of many electrons is taken into account through

$$\sigma_{INC}(\theta) = \sigma_{KN}(\theta)\, S(q,Z)$$

where $\sigma_{INC}(\theta)$ is the differential whole-atom cross section expressed as a product of the Klien–Nishima cross section $\sigma_{KN}(\theta)$ and the incoherent scattering factor $S(q,Z)$, a function of the momentum transfer q in the scattering process and the atomic number Z. According to the Thomas–Fermi statistical model (TF), which is better for heavy atoms, the scattering factor is given by Heisenberg (4). The exact TF values for S have been used for the computation of $\sigma_{INC}(\theta)$. In addition, $S(q,Z)$ values have been computed from the compilation of Hubbel *et al.* (5), based on the most accurate self-consistent field (SCF) Hatree–Fock wave function of many-electron atoms under complete exchange. The differential cross sections computed in the manner indicated above are shown in Table 1.

5. Discussion

The measured total-differential cross section at the momentum-transfer region (0.02–0.04 *mc*) is taken as the sum of the coherent Rayleigh-scattering component and the incoherent scattering component. The incoherent scattering contribution is evaluated by utilizing the incoherent scattering factor $S(q,Z)$, based on the model of the atom, and the coherent scattering component is determined by utilizing the numerical Rayleigh-scattering amplitudes obtained by the Pittsburgh group (1984). In addition to the present set of measurements, some other recent measurements (e.g., Bradley and Ghosh (6, 7) and Taylor *et al.* (8)) in the overlapping momentum-transfer region exist; if we compare these two sets of measurements, we find a general consistency between the results for common elements at the same momentum transfer. A demonstration of such consistency is given in Fig. 2, where results of measurements from Schumacher and Stoffregen (9) and Eichler and de Barros (10) at higher momentum transfers are plotted. The agreement with the theory, however, becomes poorer at smaller scattering angles. A major discrepancy exists in case of ^{73}Ta at smaller scattering angles. Similar differences have been reported by Gaspar *et al.* (11). If one seeks to explain this difference, one has to take into account the effect of the arrangement of atoms in the scatterer foil. A new set of experiments using scatterer foils prepared by different techniques is being organized by the authors of this paper. In a recent paper, Gaspar *et al.* (12) have explained this effect at angles of $\leq 20°$ in terms of the polycrystalline nature of the crystal.

Acknowledgements

The award of a teacher fellowship to S. K. Ghose by the University Grants Commission is gratefully acknowledged.

1. L. KISSEL and R. H. PRATT. Rayleigh scattering: elastic photon scattering by bound electrons in CH-11 atomic inner shell physics. *Edited by* B. Crasemann. Plenum Press, New York, NY. 1985.
2. B. SINHA, S. C. ROY, and N. CHOUDHURI. J. Phys. B, Vol. **9**, 3185 (1976).
3. L. KISSEL. UC 34A elastic photon atom scattering of 59.54 keV photons. Sandia Report SAND-84.0294. Sandia National Laboratories, Albuquerque, NM. 1984.
4. W. HEISENBURG. Phys. Z. **32**, 737 (1931).
5. J. H. HUBBEL, W. M. VEIGELE, E. A. BRIGGS, R. T. BROWN, D. T. CROMER, and R. J. HOWERTON. J. Phys. Chem. Ref. Data, **4**, 471 (1975).
6. D. A. BRADLEY and A. M. GHOSH. Nucl. Instrum. Methods, Phys. Res. Sect. A, **255**, 59 (1987).
7. D. A. BRADLEY and A. M. GHOSH. Phys. Rev. A, **33**, 191 (1986).
8. R. B. TAYLOR, P. TEANSOMPRASONG, and I. B. WITTINGHAM. Nucl. Instrum. Methods Phys. Res. Sect. A, **255**, 68 (1987); Phy. Rev. **37**, 3218 (1988).
9. M. SCHUMACHER and A. STOFFREGEN. Z. Phys. A, **283**, 15 (1977).
10. J. EICHLER and S. DE BARROS. Coherent scattering of 59.54 keV-rays by Al, Cu, Zn, Cd, and Pb. Preprint. Instituto de Fisica, Universidade Federal do Rio de Janeiro, Z.
11. M. GASPAR, O. GONÇALVES, S. DE BARROS, and J. EICHLER. 1983. Cidade Universitária, Rio de Janeiro, Brazil.
12. M. GASPAR *et al.* Phy. Rev. Abstracts, **19**, No. 7 (1988).

Lower energy photon cross sections near atomic shell edges

MANJUSREE GHOSH,[1] S. K. GHOSE, AND S. C. DAS
Department of Physics, North Bengal University, Darjeeling, West Bengal 734430, India
N. BHATTACHARYYA[2]
Cooch Behar T. and Evening College, West Bengal, India
P. CHOWDHURI
Department of Physics, North Bengal University, Darjeeling, West Bengal, 734430, India
S. K. SEN GUPTA
University Science and Instrumentation Centre, North Bengal University, Darjeeling, West Bengal 734430, India
AND
N. CHAUDHURI
Department of Physics, North Bengal University, Darjeeling, West Bengal 734430, India

Received July 13, 1989

Photon attenuation cross sections have been measured from time to time using radioactive isotopes as photon sources in various geometries. There are, however, inconsistencies between the measured values and the available tabulated values of attenuation coefficients based on different theoretical models. The measured values are particularly deficient for photon energies in the neighbourhood of the *K*-shell binding energies of attenuator elements. With the objective of filling such gaps in the experimental data as well as improving the data of earlier measurements, we have undertaken the present measurements in the energy region 43–1330 KeV. The measurements are made with the transmission technique using a NaI detector in the "good geometry," in which no gamma-ray photon scattered from the absorber at an angle greater than 0.3° can reach the detector. Results covering the elements from $Z = 6$–92 are presented and compared with the tabulated values of Hubbell *et al.* and Schaupp *et al.*

Les sections efficaces d'atténuation photonique ont été mesurées de temps en temps en utilisant des isotopes radioactifs comme des sources de photons dans des géométries variées. Il y a cependant des inconsistances entre les valeurs mesurées et les valeurs disponibles dans les tables de coefficients d'atténuation basés sur différents modèles théoriques. Les valeurs mesurées sont particulièrement déficientes pour les photons dont l'énergie est dans le voisinage des énergies de liaison de la couche *K* des éléments atténuateurs. Avec l'objectif de combler de tel vides dans les données expérimentales aussi bien que d'améliorer les données des expériences précédentes, nous avons entrepris les présentes mesures dans la gamme d'énergie allant de 43–1330 KeV. Les mesures sont effectuées par la technique de transmission utilisant un détecteur NaI dans la « bonne géométrie », où aucun photon gamma diffusé dans le matériel absorbant à un angle plus grand que 0.3° ne peut atteindre le détecteur. Des résultats couvrant les éléments de $Z = 6$–92 sont présentés et comparés avec les valeurs tabulées de Hubbell *et al.* and Schaupp *et al.*

[Traduit par la revue]

Can. J. Phys. 68, 244 (1990)

1. Introduction

The theoretical treatment and numerical computation of various photon–atom interaction processes has received a great deal of attention with modern computers in the last two decades. The treatment of photon elastic scattering from atoms using the independent particle model of the atom with the relativistic self-consistent central potential has given improved results (1–3) for many elements over a large photon-energy range simultaneously with the studies (4–7) on the effect of anomalous scattering near the inner shell edges. The status of the photon–atom inelastic scattering calculation has not reached such a standard yet. The treatment of the photo-ionization process in atoms using the relativistic Hartree–Slater atomic model has given extensive results (8) for all elements over a wide range of photon energies. However, there may exist errors in the calculation near the inner shell edges when the photo-electron receives a small amount of energy. In such a situation, in addition to the different atomic processes involved, the solid-state effects may modify the cross-section structure in the vicinity of the shell edges.

It is easy to measure precisely the cross-section structure between successive atoms in the periodic table near the absorption edges by observing the transmission of a very narrow monoenergetic photon beam of appropriate energy through thin, pure elemental samples fixed perpendicular to the photon beam. Although extensive cross-section measurements by this method have been carried out and compiled at the National Bureau of Standards (NBS) in the U.S.A. (9–11), the method is still attractive and useful from the point of view of the high precision, which is dependent mainly on the photon-counting geometry and statistics. The purpose of the present work is to examine the behaviour of the total cross section near the absorption edges as the atomic number of the interacting atom is increased. The improved results from the recent computational theories of photon–atom interaction processes guide this analysis.

2. Experimental method

The experimental arrangement used in our measurements is shown in Fig. 1. An improvement has been achieved by a high degree of collimation of the photon beam from the source to the detector. The source was placed in 10 cm deep conical bore in a lead block. The minimum thickness of the lead shielding at the side and the back of the source was 20 cm. Collimator number 1 was a 23 cm thick iron block having a collimating bore of exit aperture of 0.4 cm. The collimation of the beam after the attenuation in the target foil was provided by collimators 2 and 3, which had a total thickness of 15 cm

[1]On leave from B. K. Girl's College, Howrah, India.
[2]Guest researcher.

Printed in Canada Imprimé au Canada

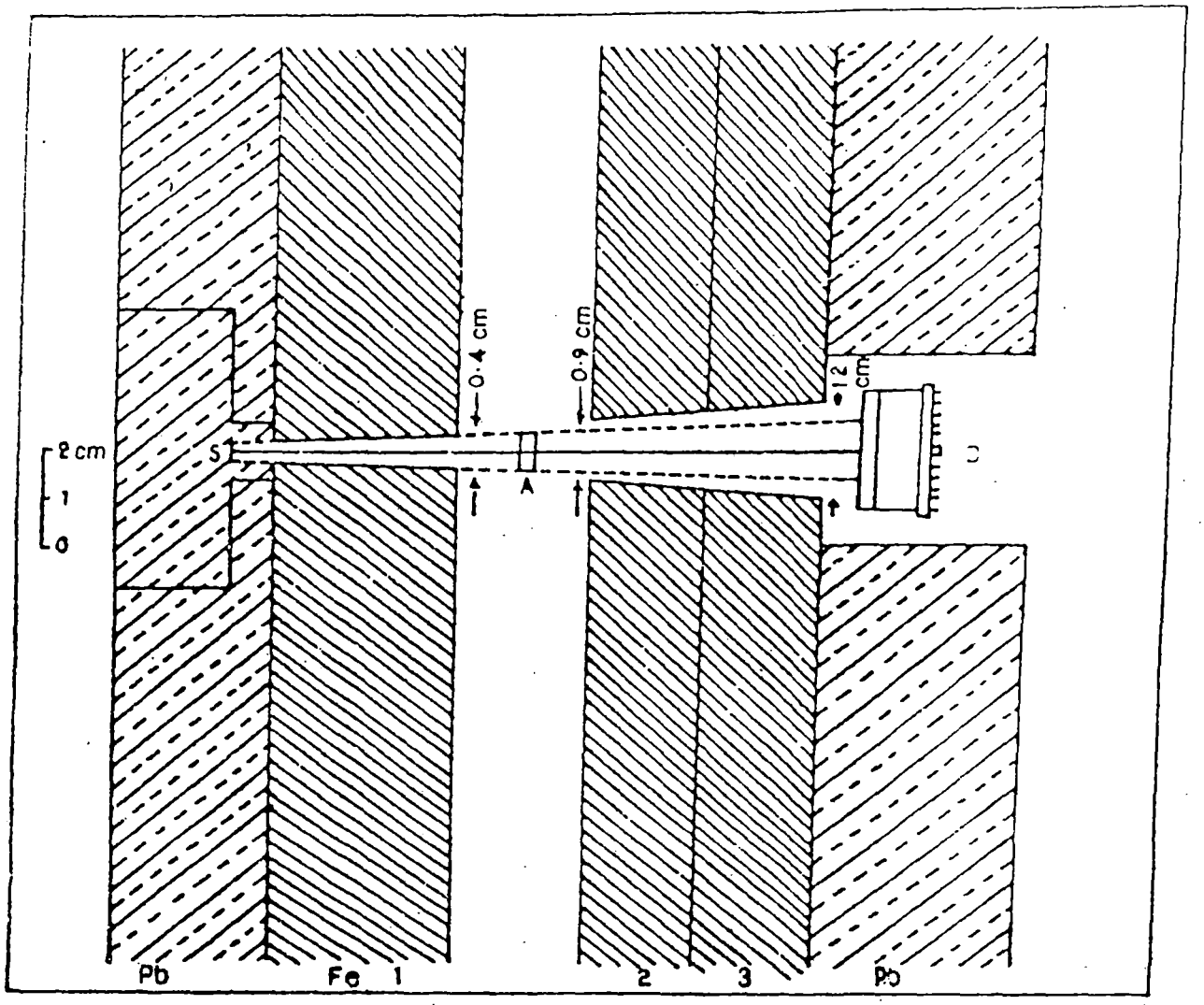

FIG. 1. Experimental arrangement. S, source; A, attenuator; D, detector.

of iron. The collimators prevented photons scattered in the air and the shield materials from reaching the detector. The collimators were mounted on a rigid bench of iron. These collimators could be moved so that measurements at two or more narrow beam geometries could be carried out after changes in the collimator apertures. In measurements carried out with the sample 20 cm from the source, the solid angle of the collimating system between the attenuator and the detector was 3.8×10^{-4} sr. In this geometry, the maximum angle of scattering from the attenuator to the detector was 0.3°. The detector, a 2.5 cm NaI (TI) scintillator, was shielded by 20 cm of lead and was coupled to a conventional system of photomultiplier preamplifier, and a Nuclear Data 1100 multichannel analyser.

3. Materials and measurements

In the present work, the photon–atom interaction cross-section measurements have been made on a pyrolytic graphite specimen and a single-crystal silicon specimen, for photon energies of 59.5, 662, 889, 1115, 1120, 1173, and 1332 KeV and on thin foil samples of rare-earth elements in the atomic number range $Z = 41$–70 and tantalum ($Z = 73$), gold ($Z = 79$), and uranium ($Z = 92$) using photon beams 43 and 59.5 KeV in energy. Most of the sample foils were supplied by Good Fellow Metals, Cambridge, England, within a purity range of 99.9 – 99.99%. Single-crystal silicon specimens were obtained from the International Union of Crystallography X-ray attenuation project. It was assumed that when a narrow beam of photons passed through an assembly of atoms in a solid in the form of a thin foil, for the photon–atom interaction the Beer–Lambert law, $I = I_0 \exp(-\mu_m X)$, connecting the incident beam intensity I_0 and the transmitted intensity I through a foil of thickness X (g · cm^{-2}), applied. Here μ_m was the mass attenuation coefficient defined by $\mu_m = \sigma N/A$, where N is Avogadro's Number, A is the atomic weight of the atom in the foil sample, and σ is the photon–atom cross section.

Measurements were carried out at good geometry, the arrangement being one involving a photon source, surrounded by appropriate shielding, and a collimator to confine the photons into a narrow beam as it impinged on the material sample. The detector was also collimated and shielded. The elemental foils, used as targets, were very thin, satisfying the condition necessary for the Beer–Lambert Law to hold. Under the steady conditions of the detector system, no drift of the photopeak was detected over at least 24 h. Countings were taken for 2×10^3 s. Background counts were observed with the source and the attenuator in position and a 20 cm long stopper placed in the beam behind the attenuator and collimators 2 and 3. Background counts were also observed with the source absent.

TABLE 1. Total photon attenuation cross sections in barns per atom

Element (Z)	Foil thickness (g/cm²)	Photon energy (KeV)	Total cross section (b/atom) Theoretical	Total cross section (b/atom) Measured	Percent deviation from theory
6[a]	(0.[illegible]	59.5	3.507(0.6382)	3.4051(0.004)	2.91
	(0.[illegible]6)	662	1.539(0.3047)	1.5371(0.004)	0.13
		889	1.3425(0.2683)	1.3417(0.002)	0.06
		1115	1.2028(0.2404)	1.1982(0.004)	0.38
		1120	1.2001(0.2399)	1.2021(0.004)	0.16
		1173	1.1727(0.2344)	1.1663(0.004)	0.55
		1332	1.0989(0.2197)	1.0985(0.002)	0.03
14[a]	(0.[illegible]266	59.5	15.1757(0.3568)	14.8430(0.014)	2.19
	0.0[illegible]167)	662	3.6048(0.1791)	3.6175(0.014)	0.35
		889	3.1409(0.1565)	3.1373(0.014)	0.12
		1115	2.8109(0.1402)	2.8157(0.009)	0.17
		1120	2.8046(0.1398)	2.8063(0.009)	0.06
		1173	2.7400(0.1367)	2.7458(0.009)	0.21
		1332	2.5664(0.1280)	2.5686(0.009)	0.09
41	0.01	43	1579.35(1.83)[a] 1630[b]	1548.38(39.01)	1.96
		59.5	631.83(1.14) 630[b]	733.40(14.96)	16.08
42	0.01	43	1725.44(1.97)[a] 1730[b]	—	—
		59.5	696.71(1.20)[a] 700[b]	686.81(1.43)	1.42
48	0.0[illegible]	43	2786.21(2.97)[a] 2750[b]	—	—
		59.5	1140.77(1.58)[a] 1200[b]	1242.13(3.92)	8.89
49	0.0[illegible]	43	2997.80(3.17)[a] 3250[b]	2767.97(53.36)	7.67
		59.5	1220.58(1.64)[a] 1333[b]	1351.78(21.73)	10.75
64	0.01	43	1504.50(2.35)[a] 1600[b]	—	—
		59.5	3135.15(3.42)[a] 3250[b]	34.60.92(3.92)	10.39
66	0.01	43	1709.68(2.56)[a] 1750[b]	1495.86(7.35)	12.51
		59.5	3466.98(3.75)[a] 3500[b]	—	—
68	0.01	43	1935.77(2.78)[a] 1900[b]	—	—
		59.5	3851.97(4.11)[a] 3750[b]	4031.59(3.89)	4.66
70	0.01	43	2181.26(3.02)[a] 2170[b]	2093.78(0.29)	4.01
		59.5	917.88(1.98)[a] 925[b]	941.20(3.45)	2.54
73	0.00[illegible]	43	2587.99(3.42)[a] 2680[b]	2621.96(39.95)	1.31
		59.5	1089.41(2.15)[a] 1150[b]	1060.50(15.02)	2.65
79	0.00[illegible]254	43	3568.78(4.39)[a] 3600[b]	3479.81(142.87)	2.49
		59.5	1492.97(2.55)[a] 1600[b]	1463.98(55.25)	1.94
92	0.01[illegible]24	43	6607.28(3.97)[a] 6200[b]	—	—
		59.5	2807.819(2.83)[a] 2580[b]	2534.46(1.98)	9.74

[a]Values obtained from the tabulations of Hubbell *et al.* (10)

[b]Values obtained from the tabulations of Schaupp *et al.* (12). Theoretical cross-section values for the elements $Z = 6$ and $Z = 14$ are obtained from the tabulations of Hubbell *et al.* (10)

TABLE 2. Photo-electric cross sections (in barns per atom) of elemental absorbers at 43 and 59.5 KeV photon energies

Element (Z)	Photon energy (KeV)	Photo-electric cross section (b/atom) Theoretical	Measured	Percent deviation from theory
41	43	1513.27(1.51)	1482.30(39.02)	2.04
	59.5	585.18(0.59)	686.75(14.99)	17.35
42	43	1656.09(1.66)	—	—
	59.5	647.92(0.65)	638.02(1.74)	1.52
48	43	2694.95(2.69)	—	—
	59.5	1077.70(1.08)	1179.06(4.09)	9.40
49	43	2902.58(2.90)	2672.75(53.38)	7.91
	59.5	1154.93(1.15)	1286.13(21.76)	11.35
64	43	1335.93(1.34)	—	—
	59.5	3022.75(3.02)	3348.52(4.24)	10.77
66	43	1528.35(1.53)	1314.53(7.82)	13.99
	59.5	3346.72(3.35)	—	—
68	43	1741.09(1.74)	—	—
	59.5	3723.54(3.72)	3903.16(4.26)	4.82
70	43	1972.51(1.97)	1885.03(2.31)	4.43
	59.5	780.85(0.78)	804.17(3.9)	2:98
73	43	2357.62(2.36)	2391.59(40.03)	1.44
	59.5	939.13(0.94)	910.22(15.14)	3.07
79	43	3291.56(3.29)	3202.59(142.90)	2.70
	59.5	1313.79(1.31)	1284.80(55.29)	2.20
92	43	6215.72(0.22)	—	—
	59.5	2556.31(0.07)	2282.96(3.45)	10.69

The difference between these two count rates of the background was very small. The source count without the attenuator in position was taken as the intensity of the incident beam. The mass attenuation coefficient was calculated from the supplied sample thickness and the transmission ratio. The mean value of the mass attenuation coefficient was calculated from the measurements repeated at the same solid angle between the attenuator and the detector for each sample. For some samples, measurements were repeated by varying the solid angle of the collimating system between the attenuator and the detector to study and eliminate, by extrapolation, the effects of the geometry of the experimental arrangement on the contribution of small-angle photon scattering.

4. Experimental results

The measured photon attenuation cross sections are given in Table 1, the derived photon-ionization cross sections, in Table 2. Most of the results are from measurements made at an attenuator-to-detector solid angle of 3.8×10^{-4} sr. A few measurements have been made at a solid angle of 11.1×10^{-4} sr. In the energy region involved in our measurements, the photo-electric effect is the dominant cause of beam attenuation. The cross sections for photo-ionization were derived by subtracting theoretically calculated values of elastic and inelastic scattering cross sections from the measured photon attenuation cross sections.

The effect of small-angle scattering of the photon on the measured attenuation coefficient is not observed in the geometry employed. Error due to multiply scattered photons from the attenuator was minimized by very narrow collimation of the transmitted beam of photons and measuring transmission for very thin sample foils.

5. Discussion

The theoretical estimates of cross sections for both elastic and inelastic scattering processes are based on the very recent

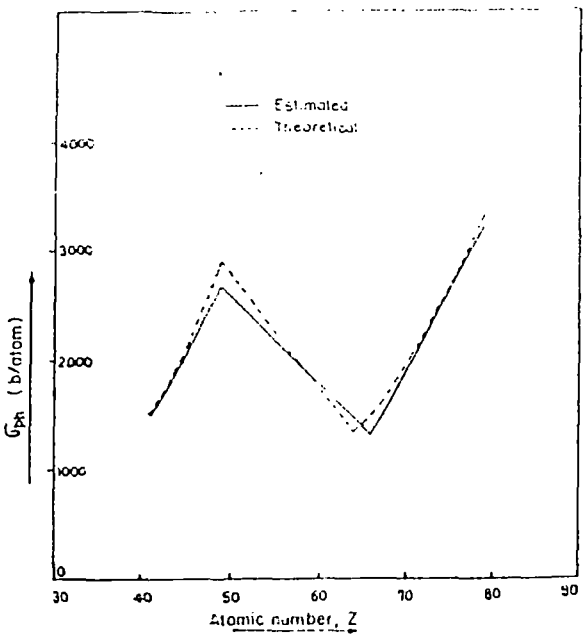

FIG. 2. Photo-ionization cross sections plotted as a function of the atomic number Z of the absorber elements at a photon energy of 43 KeV. Solid line: photo-ionization cross sections estimated from the measured photon attenuation. Coefficient; dotted line: theoretical curve.

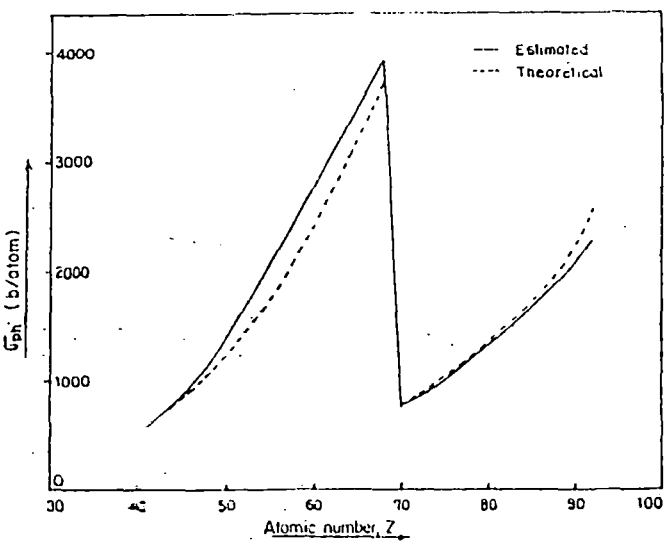

FIG. 3. Photo-ionization cross sections plotted as a function of the atomic number Z of the absorber elements at a photon energy of 59.5 keV. Solid line; photo-ionization cross sections estimated from the measured photon attenuation cross sections; dotted line: theoretical curve.

work of Schaupp *et al.* (12), Cromer–Mann and Hubell calculations (10) using Lagrangian interpolation techniques wherever necessary. Subtraction of these contributions from the measured photon interaction cross sections gives the photo-ionization cross-sections. The structures of photo-ionization cross sections at the photon energies of 43 and 59.5 KeV around the K edges of $_{60}$Nd (E_K = 43.57 KeV) and $_{90}$Th (E_K = 59.39 KeV) are shown in Figs. 2 and 3, where the measured cross sections (labelled as "estimated") are plotted together with Scofield's predictions (8). The K-edge energies (E_K) are those reported in Kaman Sciences Corporation Report KN-71-

43 (R) (13). The cross-section behaviour around the K edges has been found to be as predicted in theory.

The work presented in this paper is partly related to and has been encouraged by the International Union of Crystallography (IUCr) X-ray attenuation project, which was initiated to resolve the problems associated with the measurement of the total attenuation cross sections in the X-ray and low-energy gamma-ray region. The first report on the IUCr project indicated some problems concerning photo-effect attenuation cross sections below 100 KeV, and indicated that there has been no rational basis for preferring any one of many calculations on photo-effect cross sections (e.g., Scofield (8): Hartree–Slater and Hartree–Fock models: Cromer and Liberman (4); Storm and Israel (16); and the Dirac–Slater and Hartree–Fock–Slater models). Determination of the elastic (atomic Rayleigh) scattering and inelastic (atomic Compton) scattering, which also contribute significantly to the total photon attenuation study near resonant atomic states have also been improved (12) for higher photon energies. The problem arising from Laue–Bragg scattering and thermal diffuse scattering at energies of interest in the present work can be ignored. Consequently, we assume that the total photon attenuation cross section of an atom is due to the sum of the contributions of inelastic (Compton) scattering, elastic (Rayleigh) scattering, and the photo-effect processes, and this method of summation of individual photon–atom interaction cross sections applies to the present case where elemental sample materials in the form of thin foils have been used. Narrow-beam attenuation experiments using such technique for each photon energy and absorber foil thickness, restricted to a upper limit by the Beer–Lambert law, have been carried out.

Some of the absorber elements chosen for this experiment have K edges in the vicinity of photon energies of 59.5 and 43 KeV, filling in the gaps in the previous measurements of other workers. The present silicon measurement in the region from 59.5 to 1332 KeV has filled some gaps in the lower energy region. The comparison with Scofield's photo-effect calculations has shown some deviations from the present measurements.

The present work includes new data on six elements at photon energies of 59.5 and 43 KeV. The recommendations for such precise measurements of the total attenuation cross sections are made in the assessment of Viegele *et al.* (13). Creagh and Hubbell (14), and Saloman and Hubbell (15) in view of uncertainties in the earlier measurements as well as indistinguishability among more recent refined model calculations (7). The measurement on uranium ($Z = 92$) with 43 KeV gamma rays from ^{241}Am suffers from a deficiency arising from only 0.1% photon intensity.

Acknowledgement

The award of a Teacher Fellowship to one of the authors (S. K. Ghose) by the University Grants Commission is gratefully acknowledged.

1. W. R. Johnson and K. Cheng. Phys. Rev. A, **13**, 692 (1976).
2. L. Kissel, R. H. Pratt, and S C. Roy. Phys. Rev. A, **22**. 1970 (1980).
3. P. P. Kane, K. Kissel, R. H. Pratt, and S. C. Roy. Phys. Rep. **140**, 75 (1986).
4. D. T. Cromer and D. Liberman. Acta Crystallogr. Sect. A, Cryst. Phys. Diffs. Theor. Gen. Crystallogr. **37**, 267 (1981).
5. B. L. Henke, P. Lee, T. J. Tanaka, R. Shimabujuro, and B. K. Fujikawa. At. Data Nucl. Data Tables, **27**, 1 (1982).
6. D. C Creagh. Phys. Lett. **103A**, 52 (1984).
7. D. C. Creagh and W. J. McCauley. International Tables for Crystallography Vol. C. Sect. 4.2.6.
8. J. H. Scofield. Lawrence Livermore Laboratory Report UCRL-51326. University of California Radiation laboratory, CA. 1973.
9. J. H. Hubbell. Report NSRDS-NBS 29 (1969). National Bureau of Standards, Washington, DC. 1969.
10. J. H. Hubbell, W. J. Veigele, E. A. Briggs, R. T. Brown, D. T. Cromer, and R. J. Howerton. J. Phys. Chem. Ref. Data, **4**, 471. (1979).
11. J. H. Hubbell and I. Overbo. J. Phys. Chem. Ref. Data, **4**, 69 (1979).
12. D. Schaupp, M. Schumacher, F. Smend, P. Rullhusen, and J. H. Hubbell. J. Phys. Chem. Ref. Data, **12**, 467 (1983).
13. W. J. Viegele, E. Briggs, L. Bates, E. M. Henry, and B. Bracewell. Kaman Sciences Corporation Report KN-71-431(R). 1971. 1500 Garden of the Gods Road, Colorado Springs, CO 80907, U.S.A.
14. D. C. Creagh and J. H. Hubbell. Acta. Crystallogr. Sect. A, Found. Crystallogr. **43**, 102 (1987).
15. E. B. Saloman and J. H. Hubbell. Nucl. Instrum. Methods Phys. Res. Sect. A, **285**, 38 (1987).
16. E. Storm and H. I. Israel. Nucl. Data Tables, **7**, 565 (1970).

Experimental results on low-energy photon-atom scattering and a critical analysis of the data in the vicinity of K-absorption edges

S. K. Ghose, M. Ghose,* S. S. Nandi, A. C. Nandi, and N. Choudhuri
Department of Physics, North Bengal University, Darjeeling, West Bengal, 734 430 India
(Received 28 August 1989)

Results for the atomic elastic scattering of photons of 59.54 keV lying in the vicinity of K-absorption edges of rare earths ($_{68}$Er and $_{70}$Yb) are presented. An assessment of all existing experimental results published in the last few years has been made in terms of some of the most important calculations on photon–bound-electron collisions as a function of photon energy and momentum transfer that have been developed in the 1980s. The analysis presents the trend of behavior of the theoretical cross section as the incident photon energy crosses the K-shell photoionization thresholds of the scattering atomic system.

I. INTRODUCTION

The elastic scattering of photons in the x-ray and low-energy γ-ray regions by atomic bound electrons in the vicinity of atomic K edges has been investigated in recent years. In the energy region below 100 keV the scattering by bound electrons near the edges has been in a state of uncertainty due to problems arising from experimental techniques as well as theoretical methods. New calculations of dispersion corrections[1–4] to scattering cross sections near K edges made by a number of authors have encouraged new experimental studies on elastic photon scattering in the energy region below 100 keV. This paper includes new results for elastic photon scattering on a number of new elements with their K edges near the photon energy 59.54 keV and a critical analysis of similar experimental data published by other groups during the last few years.

II. THEORETICAL BACKGROUND

Photon-atom elastic scattering by atomic bound electrons, known as Rayleigh scattering, is expressed in the simpler atomic form factor approach by writing the differential cross section in the form

$$\frac{d\sigma^R}{d\Omega}=\frac{d\sigma^T}{d\Omega}|f(q)|^2$$

where $d\sigma^T/d\Omega=\frac{1}{2}r_0^2(1+\cos^2\theta)$, σ^R represents the photon-bound electron total scattering cross section, $r_0=e^2/mc^2$, the classical electron radius, θ is the scattering angle, $q=mcq'=2(\hbar\omega/c)\sin\theta/2$, $\hbar\omega$ is the incident photon energy, and q' is the change in photon momentum for the scattering process (i.e., momentum transferred to the atom by the scattering). The atomic form factor $f(q)$ for a spherically symmetric atom is given by

$$f(q)=4\pi\int_0^\infty \rho(r)\frac{\sin(qr)}{(qr)}r^2dr$$

where $\rho(r)$ is the charge number density satisfying the condition

$$4\pi\int_0^\infty \rho(r)r^2dr=1\ .$$

If the elastic scattering is due to a photon of energy very close to the atomic energy level, photon-resonant scattering will occur. The scattering power of the atom represented by $f(q)$ has to be modified by two correction terms, one arising from the proximity of the incident photon energy to the binding energy of the bound electron scattering the photon, and the second one representing absorption due to damping of the incident photon in the vicinity of the resonance level. With these two correction terms the true atomic scattering factor is written as

$$f_{\text{true}}=f(q)+f'+if''\ ,$$

where $f(q)$ is the atomic scattering factor far from any resonant bound electron energy level. f' is a real number representing the dispersion effect in scattering near the resonant level and if'' is an imaginary number representing the absorptive part of the dispersion effect in elastic scattering near a resonant state of the bound scattering electron.

III. WORK ON DISPERSION EFFECTS IN ELASTIC PHOTON SCATTERING

The initial work in the x-ray regime has been summarized by Compton and Allison in their book[5] which was extended to include the work of Honl.[6] In the extension of Honl's work, the real and imaginary parts of the dispersion correction (denoted by f' and f'') were predicted to depend on the photon frequency and momentum transfer as the following:

$$f_{\text{true}}(\omega,q)=f(\omega,q)+f'(\omega,q)+if''(\omega,q)\ .$$

However, the momentum transfer dependence had not been tested experimentally and more recent theoretical treatments do not support the predictions of Wagenfeld,[7] that f' and f'' are dependent on the momentum transfer. The determination of the dispersion corrections for the

case with $q \neq 0$ is based on the following relationships obtained in the dipole approximation:

$$f'' = \frac{\omega}{4\pi r_0 c}\sigma_{Ph}(\omega), \quad f' = \frac{1}{2\pi^2 r_0 c} P \int_{\omega_k}^{\infty} \frac{\omega'^2 \sigma_{Ph}(\omega')}{\omega^2 - \omega'^2} d\omega' ,$$

where $\sigma_{Ph}(\omega)$ is the photoelectric cross section, ω is the photon angular frequency, ω' is the angular frequency corresponding to the bound electron atomic level, c is the velocity of light, and P refers to the principal value of the integral.

The relativistic calculation of dispersion corrections f' and f'', based on the Dirac-Slater model calculation of photoelectric cross sections, were found by experiments to be inadequate. Cromer and Liberman,[1-3] however, have published improved calculations based on the Dirac-Hartree-Fock-Slater (DHFS) model.

The scattering matrix formalism of Brown and Meyers[8] and Kissel, Pratt, and Roy[9] using the DHFS model have provided extensive numerical calculations of whole-atom photon–bound-electron elastic scattering cross sections and also have given two schemes for applying dispersion corrections $f'(\omega,0)$ and $f''(\omega,0)$ at scattering angles with nonzero momentum transfer ($q \neq 0$). The method for applying $f'(\omega,0)$ and $f''(\omega,0)$ at higher scattering angles ($q \neq 0$) has not been tested. The present paper will test the predictions of Kissel and Pratt as well as very recent results of dispersion corrections[4] for an assessment in terms of recent experiments done over the last few years.

IV. PRESENT AND OTHER RECENT EXPERIMENTS

A sensitive intrinsic germanium detector (crystal specifications: 100-mm^2 active area, 7-mm thickness, 3.5-mm distance from detector to crystal window face) has been used for precision measurements of the photon-atom interaction replacing the previous NaI detector system because the resolution of the present detector system has been improved to 176 eV [full width at half maximum (FWHM)] for a photon energy of 5.89 keV. These improvements helped carry out measurements with an accuracy at the level of 5%. The experiments were carried out using a 10-mCi ^{241}Am source which emits γ rays with an energy of 59.54 keV. With this source a very accurate determination of the number of elastically scattered photons is possible, as these are well separated in the scattered spectrum from the component of inelastically scattered photons. The ^{241}Am source was placed in a lead shield housing of an adequate thickness permissible by the geometry at each angle in order to minimize the background reading. The housing has a conical bore with a length of 30 cm and a diameter of 2 cm as shown in Fig. 1. The angle of scattering (θ) and the angle (ψ) between the direction of incident beam and the scatterer were measured very carefully and accurately each time by telescopic arrangement. Each setting was checked to adjust the source, the scatterer, and the detector in the same horizontal plane. Background reading (without the scatterer at the scatterer holder) was always taken before and after each measurement. The average background

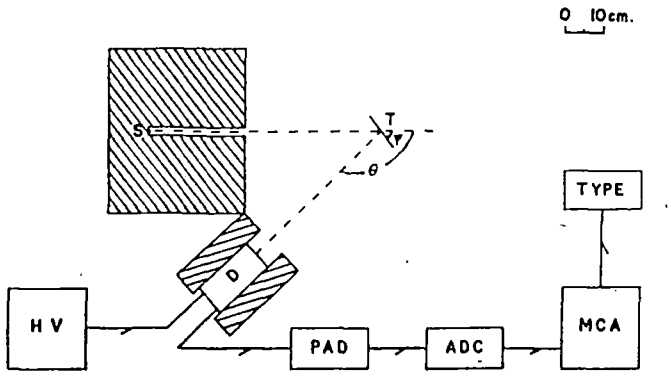

FIG. 1. Schematic diagram of the experimental arrangement S, source; T, target; D, detector; HV, high voltage; PAD, pulse amplitude discriminator; ADC, analog-to-digital converter; MCA, multichannel analyzer.

result was subtracted from the reading obtained with the scatterer at the position of the scatterer holder. The position of the particular channels in the multichannel analyzer (MCA) in which the coherent component peak appeared was tested before and after the experiment to check for any channel shift. The distance (r_1) between the source and the scatterer and the distance (r_2) between the scatterer and the detector were always kept equal. Simultaneously, the relation between θ and ψ was always $\psi = \theta/2$. These two adjustment were done to satisfy the condition

$$\frac{r_1}{r_2} = \frac{\sin\psi}{\sin(\theta - \psi)} .$$

The target foils used have the following dimensions.

Target atom	Area (cm^2)	Thickness (cm)
Mo	25	0.01
Cd	25	0.005
Sn	19.63	0.01
Er	25	0.01
Yb	25	0.01
Ta	19.63	0.001

Measurements were made using an ND 1100 multichannel analyzer system coupled to a Ge-detector head at a conversion gain of 1024 with 512 channels and a spectrum storage time in the range 4–100 ks. At a large scattering angle θ, the expression for the differential elastic scattering cross section can be shown to be

$$\frac{d\sigma}{d\Omega} = \frac{4\pi N_s \sin\theta r_1^2 r_2^2}{N_{at} I_0 \epsilon A_d} G(\theta) \qquad (1)$$

where N_{at} is the number of scattering atoms in the target, N_s is the number of scattered photons per second (scattered into the infinitesimal solid angle $d\Omega$), I_0 is the number of monoenergetic photons that the source emits per second, A_d is the area of the detector, and $G(\theta)$ is the geometrical correction factor (obtained from Kahane, Bar-Noy, and Moreh[10]). For relection geometry

$$G(\theta) = \frac{1 - e^{-\mu t[1/\sin\psi - 1/\sin(\theta-\psi)]}}{\mu t[1/\sin\psi - 1/\sin(\theta-\psi)]}$$

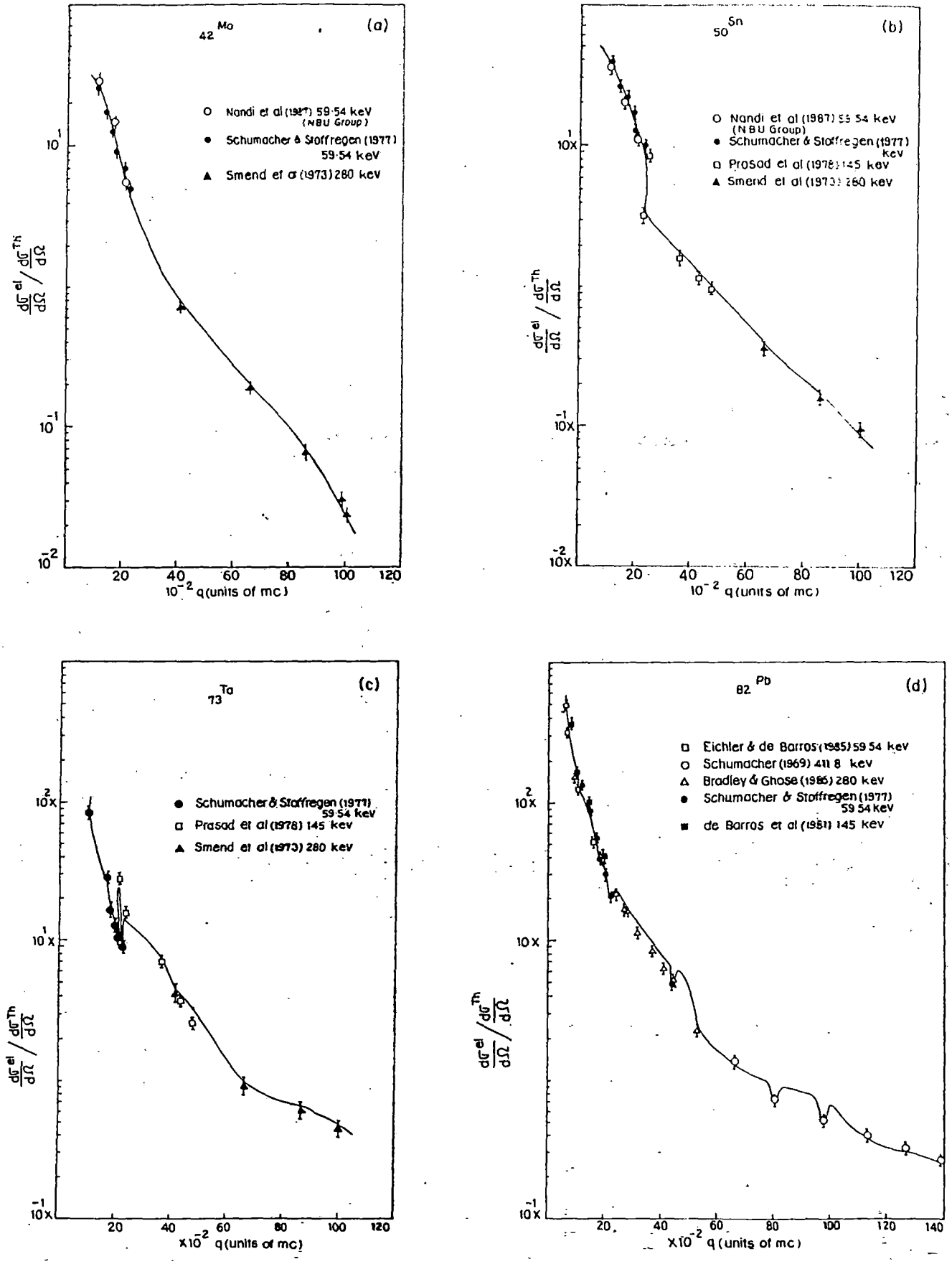

FIG. 2. Plot of $(d\sigma^{el}/d\Omega)/(d\sigma^{T}/d\Omega)$ against momentum transfer q in units of mc (a) for $Z=42$, (b) for $Z=50$, (c) for $Z=73$, and (d) for $Z=82$. The theoretical S-matrix predictions are plotted with the solid line and the experimental data points are shown by the symbols under the references as listed.

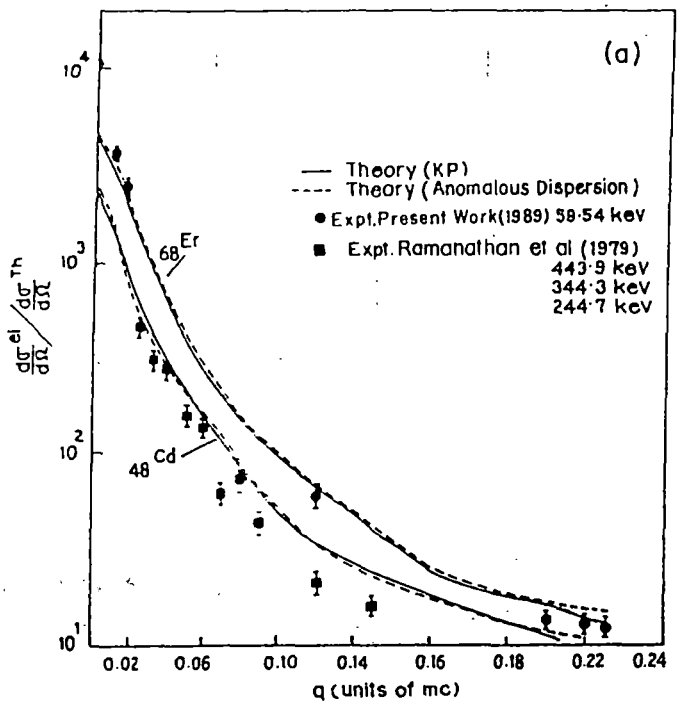

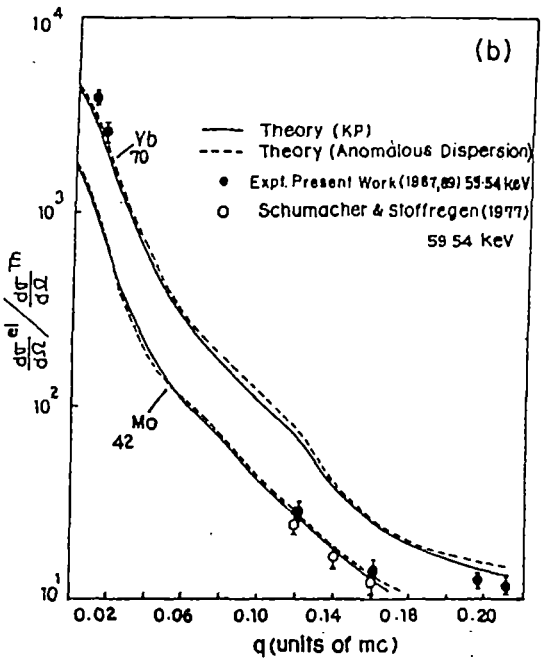

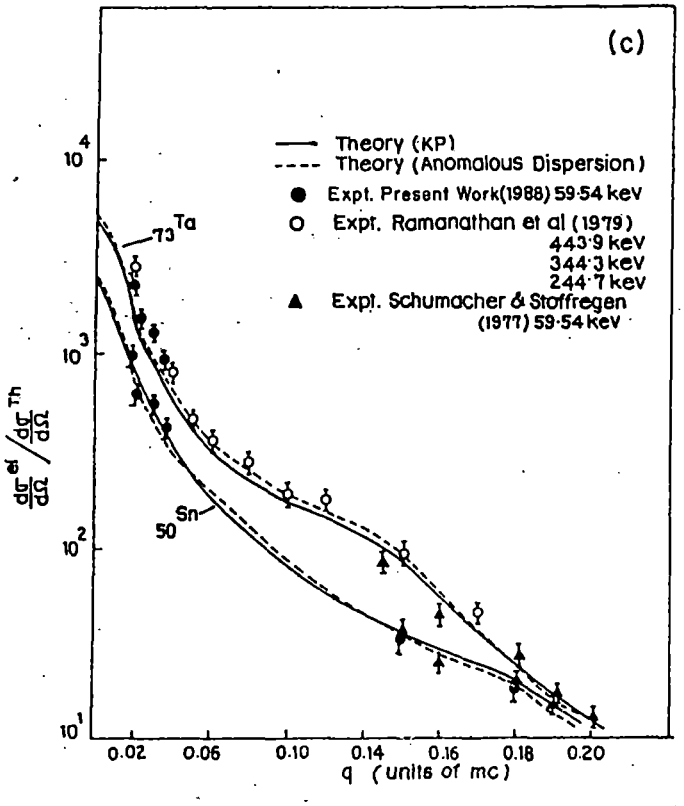

FIG. 3. Plot of $(d\sigma^{el}/d\Omega)/(d\sigma^{T}/d\Omega)$ aganst momentum transfer q in units of mc (a) for $Z=48$ and $Z=68$, (b) for $Z=42$ and $Z=70$, and (c) for $Z=50$ and $Z=73$. The theoretical S-matrix predictions are plotted with the solid line and the values obtained by using relativistic form factor corrected by anomalous dispersion terms of Creagh and McAuley are plotted with the dashed line. The experimental data points are shown by the symbols under the references as listed.

where μ (cm^{-1}) is the attenuation coefficient of the scatterer atom for incident photons and t (cm) is the thickness of the scatterer. An auxiliary experiment was carried out to determine the direct photon beam counts by keeping the intrinsic Ge detector at a large distance R. The direct photon beam count N_{Ge} is used in the formula connecting the source strength and the detector parameter expressed as

$$N_{Ge}=\frac{I_0}{4\pi R^2}A_d\epsilon\,. \tag{2}$$

When the result is compared with formula (1), the product $I_0\epsilon A_d$ is eliminated. In this way the determination of the efficiency (ϵ), source strength (I_0), and the detector area (A_d) was avoided.

Such high-resolution photon-atom scattering work in similar scattering geometry carried out during the last few years includes the work of Schumacher,[11] Smend, Schumacher, and Borchert,[12] Schumacher and Stoffregen,[13] Prasad *et al.*,[14] Ramanathan, Kennett, and Prestwich,[15] de Barros *et al.*,[16] Eichler and de Barros,[17] and Bradley and Ghose.[18] Bradley and Ghose, however,

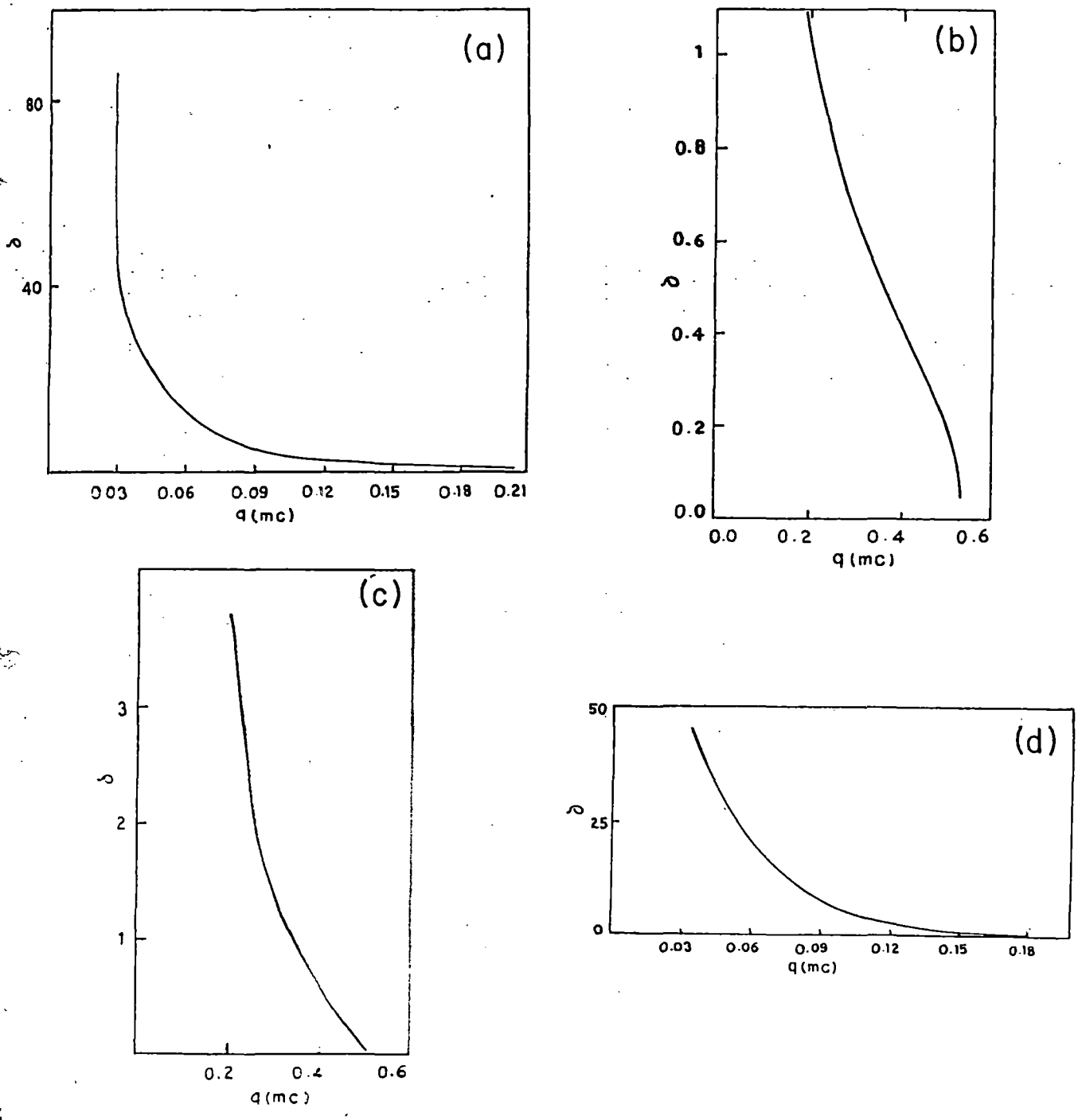

FIG. 4. Deviation δ of the experimental cross sections in units of $d\sigma^T/d\Omega$ from the corresponding theoretical values plotted against q in units of mc (a) for $Z=82$ with $E/E_k=0.675$, (b) for $Z=82$ with $E/E_k=3.17$, (c) for $Z=82$ with $E/E_k=4.679$, (d) for $Z=73$ with $E/E_k=0.883$, and (e) for $Z=50$ with $E/E_k=11.78$.

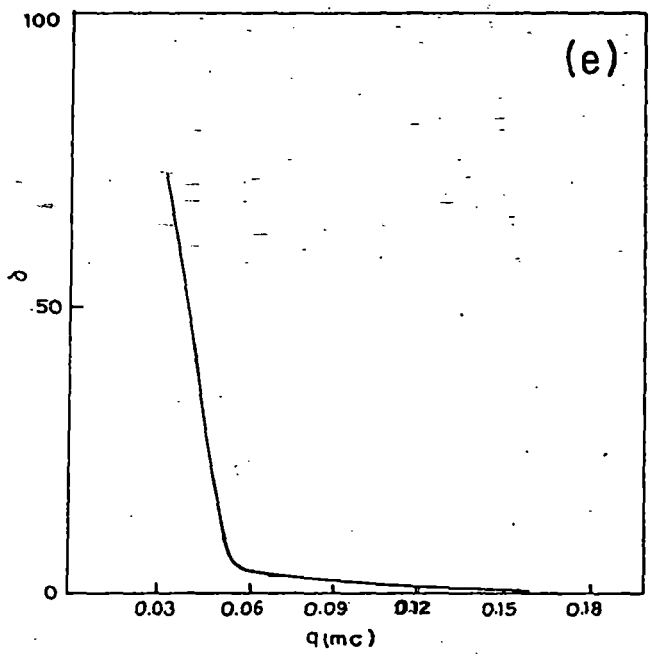

FIG. 4. (*Continued*).

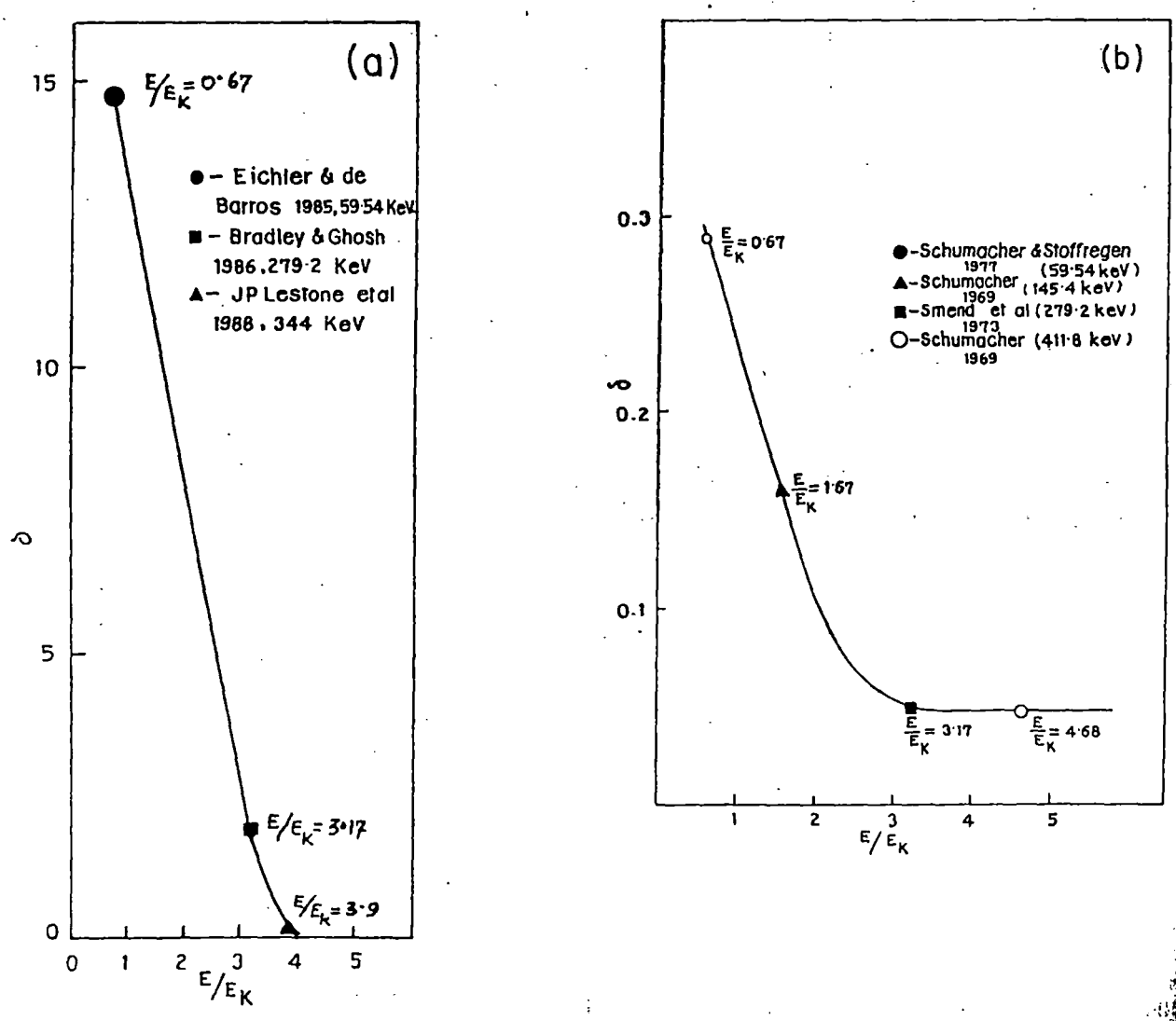

FIG. 5. Plot of δ against E/E_k for $Z=82$ (a) at the scattering angle $\theta=20°$ and (b) at the scattering angle $\theta=150°$.

ave used scatterers in the shape of a surface of revolution about the source-detector axis. Lestone *et al.*[19] have performed elastic scattering measurements at angles between 2° and 45° using a polyenergetic γ-ray source containing ^{152}Eu and ^{154}Eu. At the small angles used in this investigation the elastic scattering peak and Compton peak overlap. The relative intensities of elastic and Compton scattering of a photon at an angle were therefore extracted using a least-squares method based upon experimentally measured Compton and elastic line shapes. Absolute elastic scattering cross sections were obtained using theoretical Compton cross sections for carbon (by normalizing to the theoretical carbon Compton cross section at 7°).

V. RESULTS AND DISCUSSION

For the analysis intended in this paper, we have presented the cross-section results from the set of complete measurements performed at a photon energy of 59.54 keV and have also included the experimental data of several other groups who have used high-resolution detection systems for other energies and scatterers: Schumacher[11] for 411.8 keV, Smend, Schumacher, and Borchert[12] for 280 keV, Ramanathan, Kennett, and Prestwich[15] for 244.7, 344.3, and 443.9 keV, de Barros *et al.*[16] for 145 keV, Eichler and de Barros[17] for 59.5 keV, Bradley and Ghose[18] for 280 keV, and J. P. Lestone *et al.*[19] for 344 keV. The cross-section data obtained from these experiments are compared with those predicted by theory in Figs. 2 and 3. The error bars on the data points include both systematic and statistical errors. In these graphs, the cross-section values have been expressed in units of Thomson cross section per electron and plotted as a function of the momentum transfer q in units of mc. The examination of the cross section as a function of momentum transfer allowed the experimental data of other groups on common targets to be considered even though the photon energies employed and the range of scattering angles investigated were different.

Some of the theoretical calculations (Kissel and coworkers,[9,20] Cromer and Liberman,[1-3] Wagenfeld,[7] and the most recent calculations of dispersion corrections by

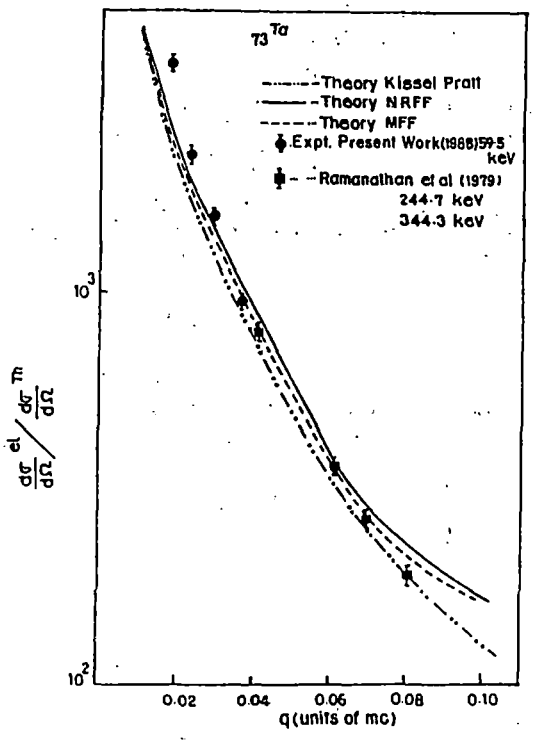

FIG. 6. Plot of $(d\sigma^{el}/d\Omega)/(d\sigma^{T}/d\Omega)$ against momentum transfer q in units of mc for $Z=73$. Theoretical predictions: nonrelativistic form factor (solid line), modified form factor (dashed line), and numerical Kissel-Pratt (dash-dotted line). Experimental points: 59.5 keV, Present Work (1988); 244.7 keV and 344.3 keV, Ramanathan, Kennett, and Prestwich (Ref. 15).

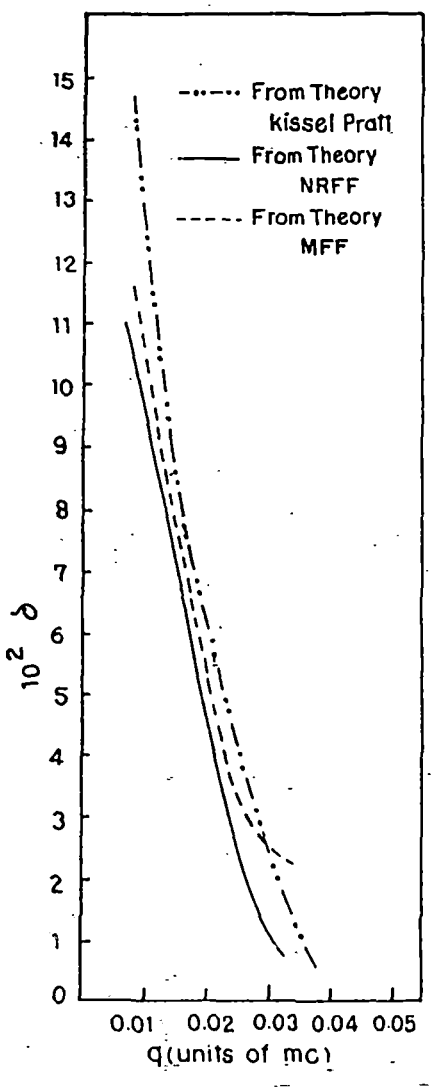

FIG. 7. Deviation δ of experimental $(d\sigma^{el}/d\Omega)/(d\sigma^{T}/d\Omega)$ from the corresponding theoretical values plotted against q in units of mc. The solid line denotes from nonrelativistic form factor, the dashed line denotes from modified form factor, and the dash-dotted line denotes from numerical Kissel-Pratt theory.

Creagh and McAuley[4]) include the corrections for the dispersion effect in photon-bound electron scattering. In Figs. 2 and 3 we have used only two theoretical models for comparison: the numerical S-matrix calculations of Kane *et al.*[21] and the relativistic form-factor calculations corrected for forward angle dispersion terms obtained from the calculations of Creagh and McAuley.[4] The computations of Kane *et al.* (referred to as the S-matrix formalism) are based on the exact numerical partial-wave method with the independent electron model. The simpler form-factor computation utilizes the atomic form factors obtained from the tabulations of Hubbell and Overbo[22] and the real and imaginary parts of dispersion corrections (f' and f'') as derived by Creagh and McAuley[4] based on attenuation measurements.

The dependence of the deviation δ of the experimental cross section from the corresponding theoretical value (both expressed in units of the Thomson cross section per electron) on the momentum transfer q (in mc units) is shown in Fig. 4 for each of the several E/E_k (the ratio of the incident photon energy to the target K-edge energy) values. In Figs. 5(a) and 5(b), on the other hand, values have been plotted against E/E_k for the scattering angles 20° and 150°, respectively. In the δ versus q graphs, however, we have not included all the cross-section results of measurements mentioned earlier. With a view to examining the data points with reference to the respective E/E_k values in the different regions of the q distribution we have chosen the experimental data from the results of measurements by various groups corresponding to a few representative q values from different regions. No attempt has been made to eliminate anomalous data sets.

We have further examined the simpler form-factor theories for the description of the elastic (Rayleigh) scattering of photons by the low-, medium-, and high-Z atoms by using (i) the calculations of Hubbell *et al.*[13] based on nonrelativistic Hartree-Fock wave functions and (ii) the calculations of Schaupp *et al.*[24] based on relativistic Dirac-Hartree-Fock-Slater wave functions. We find that for low- and medium-Z atoms and in the high-q range the distribution of $d\sigma/d\Omega$ is in good agreement with the nonrelativistic and modified form-factor results which are nearly the same as the results of numerical Kissel-Pratt calculations. But for scattering by high-Z atoms in the high-q region, the experimental results agree with the Kissel-Pratt predictions and differ considerably from both nonrelativistic and modified form-factor theories. The situation with respect to the two form-factor theories and the Kissel-Pratt predictions in the low-q range for $Z=73$ is displayed in Figs. 6 and 7.

An examination of the graphs reveals the following general trends.

(i) For incident photon energies above the K edges of target atoms ($E/E_k > 1$), theoretical predictions in different formalism appear to be in close agreement. The experimental results included in this analysis are generally in accord with theory.

(ii) At photon energies with E/E_k greater than 1 and in the momentum transfer range beyond $q=0.1$ the data points show better agreement with the various predictions of theory.

(iii) The experimental data exhibit larger deviations from theory for E/E_k less than 1 and at momentum transfer q below 0.1.

(iv) The points with E/E_k greater than 1 and at backward scattering angles agree reasonably well with theory. Significant deviations from theory seem to occur at forward scattering angles, particularly for E/E_k less than 1.

(v) At photon energies very nearly equal to the K-edge energy (i.e., $E/E_k \simeq 1$) experimental data are lacking. Elastic scattering measurements on $_{68}$Er ($E_k=57.49$ keV) using 59.54-keV photons at angles of 60°–150° showed that the cross-section results were 5–15 % lower than the S-matrix predictions over the whole range of scattering angles. Kane *et al.*[25] have reported measurements on $_{82}$Pb ($E_k=88.001$ keV) with 88.03-keV photons at the angle 125°. They obtained a cross-section value which is about 40% larger than the value predicted by S-matrix calculations.

We plan to examine the behavior of photon differential cross section on the vicinity of threshold energy positions in medium- and high-Z elements in future work.

ACKNOWLEDGMENTS

Support to S. K. Ghose by the University Grants Commission, India, is gratefully acknowledged.

*On leave from B. K. Girls' College, Howrah, West Bengal, India.

[1]D. T. Cromer and D. Liberman, J. Chem. Phys. 53, 1891 (1970).
[2]D. T. Cromer and D. Liberman, Acta Crystallogr. Sect. A 37, 267 (1981).
[3]D. T. Cromer and D. Liberman, J. Appl. Crystallogr. 16, 437 (1983).
[4]D. C. Creagh and W. J. McAuley, *International Tables for Crystallography* (Kynoch, Birmingham, in press), Vol. C 4.2.6.
[5]X. Compton and X. Allison, *X-rays in Theory and Experiment* (Van Nostrand, New York, 1935).
[6]H. Honl, Ann. Phys. (Leipzig) 18, 42 (1933).
[7]H. Wagenfeld, *Anomalous Scattering*, edited by S. Ramaseshan and S. C. Abrahams (Mankasgaard, Copenhagen, 1975), pp. 12–23.
[8]G. E. Brown and D. F. Meyers, Proc. R. Soc. London, Ser. A 234, 387 (1955).
[9]L. Kissel, R. H. Pratt, and S. C. Roy, Phys. Rev. A 22, 1970 (1980).
[10]S. Kahane, T. Bar-Noy, and R. Moreh, Nucl. Phys. A 280, 180 (1977).
[11]M. Schumacher, Phys. Rev. 182, 7 (1969).
[12]F. Smend, M. Schumacher, and I. Borchert, Nucl. Phys. A 213, 309 (1973).
[13]M. Schumacher and A. Stoffregen, Z. Phys. A 283, 15 (1977).
[14]M. S. Prasad, G. K. Raju, K. N. Murty, V. A. N. Murty, and V. Lakshminarayana, J. Phys. B 11, 3969 (1978).

[13]N. Ramanathan, T. J. Kennett, and W. V. Prestwich, Can. J. Phys. 57, 343 (1979).
[16]S. de Barros, J. Eichler, M. Gaspar, and O. Goncalves, Phys. Rev. C 24, 1765 (1981).
[17]J. Eichler and S. de Barros, Phys. Rev. A 32, 789 (1985).
[18]D. Bradley and A. M. Ghose, Phys. Rev. A 33, 191 (1986).
[19]J. P. Lestone, R. B. Taylor, P. Teamsomprasang, and I. Whittingham, Phys. Rev. A 37, 3218 (1988).
[20]L. Kissel and R. H. Pratt, Lawrence Livermore Laboratory Report No. XRM-78-107 (1978), unpublished.
[21]P. P. Kane, L. Kissel, R. H. Pratt, and S. C. Roy, Phys. Rep. 140, 75 (1986).
[22]J. H. Hubbell and I. Overbo, J. Phys. Chem. Ref. Data 8, 69 (1979).
[23]J. H. Hubbell, W. J. Veigele, E. Briggs, R. T. Brown, and D. T. Cromer, J. Phys. Chem. Ref. Data 4, 471 (1975).
[24]D. Schaupp, M. Schumacher, F. Smend, P. Rullhusen, and J. H. Hubbell, J. Phys. Chem. Ref. Data 12, 467 (1983).
[25]P. P. Kane, G. Basavaraju, Saharsha M. Lad, K. M. Varier, L. Kissel, and R. H. Pratt, Phys. Rev. A 36, 5626 (1987).